Published in final edited form as:

Cytoskeleton (Hoboken). 2019 April ; 76(4): 322–336. doi:10.1002/cm.21547.

Functional importance of an inverted formin C-terminal tail at morphologically dynamic epithelial junctions

Anna Hegsted[†,§], **SarahBeth Votra**[†,¶], **Amylisa M. Christophe**[‡,††], **Curtis V. Yingling**[†], **Sumana Sundaramurthy**[†], **David Pruyne**[†,‡‡]

[†]Department of Cell and Developmental Biology, SUNY Upstate Medical University, Syracuse, NY

[‡]Department of Clinical Laboratory Sciences, SUNY Upstate Medical University, Syracuse, NY

[§]Present address: Department of Integrative Biology, University of Wisconsin-Madison, Madison, WI

[¶]Present address: Department of Ophthalmology, SUNY Upstate Medical University, Syracuse, NY

[††]Present address: College of Medicine, MD Program, SUNY Upstate Medical University, Syracuse, NY

Abstract

Epithelial cell-cell junctions have dual roles of accommodating morphological changes in an epithelium, while maintaining cohesion during those changes. An abundance of junction proteins have been identified, but many details on how intercellular junctions respond to morphological changes remain unclear. In *Caenorhabditis elegans*, the spermatheca is an epithelial sac that repeatedly dilates and constricts to allow ovulation. It is thought that the junctions between spermatheca epithelial cells undergo reversible partial unzipping to allow rapid dilation. Previously, we found that EXC-6, a *C. elegans* protein homolog of the human disease-associated formin INF2, is expressed in the spermatheca and promotes oocyte entry. We show here that EXC-6 localizes toward the apical aspect of the spermatheca epithelial junctions, and that the EXC-6-labeled junction domains “unzip” and dramatically flatten with oocyte entry into the spermatheca. We demonstrate that the C-terminal tail of EXC-6 is necessary and sufficient for junction localization. Moreover, expression of the tail alone worsens ovulation defects, suggesting this region not only mediates EXC-6 localization, but also interacts with other components important for junction remodeling.

Keywords

epithelial cells; intercellular junctions; ovulation; *Caenorhabditis elegans*; formins

[‡‡]Corresponding author.

Introduction:

Epithelial cell-cell junctions are involved in many processes, including establishing cell polarity, providing structural cohesion, and regulating water and solute passage. Of special interest is their ability to maintain epithelium cohesion during dramatic morphological changes, as during organ formation, urinary bladder filling/emptying, and skin movements. One family of cytoskeletal regulatory proteins sometimes found at cell-cell junctions is the formins (reviewed in Grikscheit and Grosse, 2016). Formins typically promote actin filament nucleation and elongation, working mainly through conserved formin homology (FH) 1 and 2 domains, and many formins can additionally bundle actin filaments, sever actin filaments, and/or stabilize microtubules (reviewed in Goode and Eck, 2007; Breitsprecher and Goode, 2013). Thus, formins are well positioned to modulate junction stability and morphology by regulating the junction-associated cytoskeleton.

Of clinical significance, the human formin encoded by the gene *inverted formin 2* (*INF2*) associates with epithelial junctions in podocytes, a specialized kidney epithelial cell (Brown et al., 2010). These junctions are essential components of the filtration barrier responsible for retaining plasma proteins during glomerular filtration. Notably, *INF2* mutations have been associated with focal segmental glomerulosclerosis (Brown et al., 2010; Boyer et al., 2011), a disease that targets podocytes and disrupts this filtration barrier (Jefferson and Shankland, 2014). However, the mechanisms by which INF2 associates with junctions, and what roles it plays there, remain unclear.

INF2 belongs to the so-called “inverted formin” subgroup of the formin superfamily (reviewed in Hegsted et al., 2017). Based on sequence homology, two *INF2*-related inverted formins are encoded in the simple genetic model organism *Caenorhabditis elegans* by the genes *excretory canal defective-6* (*exc-6*) and *inverted formin/formin three homolog-2* (*inft-2*) (Pruyne, 2016). Pointing to conservation of functionality between mammalian INF2 and worm EXC-6 formin proteins, excretory canal defects caused by an *exc-6* loss-of-function mutation can be partially rescued by expression of mutationally activated INF2 (Shaye and Greenwald, 2015). Although there are no obvious analogs to podocyte epithelial junctions in the worm excretory canal, we have shown that a functional EXC-6/green fluorescent protein (GFP) fusion is strongly associated with epithelial junctions in the spermatheca (Hegsted et al., 2016).

In *C. elegans* hermaphrodites, two sac-like spermathecae serve as receptacles that store sperm and receive oocytes during ovulation (Ward and Carrel, 1979; McCarter et al., 1999). With onset of ovulation, the distal neck of the spermatheca dilates over the course of approximately one minute to receive the large incoming oocyte from the proximal gonad arm. After oocyte entry, a resident sperm fertilizes the oocyte. The spermatheca subsequently contracts through the action of actin-rich contractile bundles, and expels the fertilized egg through the spermatheca-uterine valve and into the uterus over the course of approximately two minutes (McCarter et al., 1999). During a worm’s lifetime, each spermatheca undergoes this rapid cycle of morphological change approximately 150 times (McCarter et al., 1999). We previously demonstrated that worms bearing the mutation *exc-6(gk386)* are partially defective for the timely entry of oocytes into the spermatheca

(Hegsted et al., 2016). Here, we explore the nature of the *gk386* mutation, characterize the sub-junction distribution of EXC-6, and demonstrate the ability of this junctional domain to unzip in response to oocyte entry.

Results:

Endogenous EXC-6 associates with the pleated septate junctions of the spermatheca.

We previously demonstrated that a functional GFP-tagged EXC-6 (EXC-6::GFP) is expressed in the spermatheca, where it localizes to epithelial cell-cell junctions and occasionally along basal filamentous actin (F-actin)-rich bundles in the epithelial cells (Hegsted et al., 2016). To determine whether endogenous EXC-6 localizes the same, or if these localizations are artifacts of tagging or overexpression, we stained dissected hermaphrodite gonads with a polyclonal antibody that was raised against the EXC-6 FH2 domain (Mi-Mi et al., 2012). In EXC-6::GFP-expressing worms, EXC-6 immunostain colocalizes with GFP fluorescence, appearing as curly ribbons demarcating convoluted junctions, and more rarely along basal F-actin bundles (Figure 1 A). Line scans across spermatheca junctions in confocal micrographs show the particularly close correspondence between immunostain and GFP fluorescence at the junctions (Figure 1 A). In gonads of non-transgenic worms, EXC-6 immunostain of basal bundles was nearly undetectable, but spermatheca junctions were prominently stained (Figure 1 B). Confirming specificity of the immunostain, the junction-associated signal was absent from worms in which *exc-6* expression was knocked down through whole-worm RNAi, or from animals bearing the mutation *exc-6(gk386)* (Figure 1 B). Thus, endogenous EXC-6 in the spermatheca is primarily associated with cell-cell junctions, and localized formin is absent from *exc-6(gk386)* mutants.

The junctions between spermatheca epithelial cells are complex, with three layers: a basally positioned smooth/continuous septate junction, a medially positioned adherens junction, and an apically positioned pleated septate junction (Lints and Hall, 2009). To determine which layer EXC-6 occupies, we compared EXC-6 immunostain with the localization of six known junctional proteins tagged with GFP (Figure 2) that were previously validated to be functional and/or reproduce endogenous protein distributions (Köppen et al., 2001; McMahon et al., 2001; Simske et al., 2003; Nance et al., 2003; Anderson et al., 2008; Achilleos et al., 2010). In favorable views, EXC-6 frequently appeared apically positioned relative to the smooth/continuous septate junction proteins AJM-1::GFP and DLG-1::GFP (Köppen et al., 2001; McMahon et al., 2001; Lints and Hall, 2009), as well as to the adherens junction proteins VAB-9::GFP and HMR-1::GFP (Costa et al., 1998; Simske et al., 2003) (Figure 2). MEL-11 was reported to localize to the pleated septate junctions based on the observation that it is positioned apical to AJM-1 and to VAB-9 (Simske, 2013), suggesting EXC-6 also localizes to the pleated septate junctions. However, we were unable to compare the junction-associated localizations of EXC-6 and MEL-11::GFP (Wissmann et al., 1999) due to a strong nuclear localization for MEL-11::GFP that obscured its junction-associated signal. Instead, PAR-3::GFP and PAR-6::GFP, which associate with the apical surface of spermatheca epithelial cells (Aono et al., 2004), also partially localized in curly ribbon-like patterns similar to junction-associated EXC-6 (Figure 2), suggesting those

markers also associate with the apical-most aspect of the junctions, presumably the pleated septate junction (Lints and Hall, 2009). EXC-6 showed strong overlap with those two apical markers (Figure 2).

To more quantitatively analyze the relative apical/basal positions of EXC-6 and these markers, fluorescence intensities of EXC-6 immunostain and GFP in these animals were measured over basal-to-apical line scans of junctions viewed in confocal cross sections (Figure 3 A), and the distances between maximal immunostain and GFP fluorescence signals were measured (Figure 3 B, Table 1). As expected, smooth/continuous septate junction markers trended toward being the most basally positioned, while PAR-3::GFP and PAR-6::GFP trended toward being the most apical, and adherens junctions markers trended toward being intermediate between these (Figure 3 B). For the apical markers, PAR-6::GFP trended toward being somewhat more basal to PAR-3::GFP, but the significance of this difference is unclear. In comparison to all these, maximal EXC-6 immunostain trended toward being apical relative to the smooth/continuous septate and the adherens junction markers, and somewhat basal relative to PAR-3::GFP, but showed no apical or basal trend relative to PAR-6::GFP (Figure 3, Table 1). Thus, EXC-6 localizes to an aspect of the spermatheca junctions apical to the adherens junctions, most likely the pleated septate junctions.

To determine whether EXC-6 is required to localize any of these junctional proteins, we knocked down *exc-6* by RNAi in all these strains. We confirmed elimination of EXC-6 immunostain, but observed no difference in any of the fusion proteins (Supplementary Figure S1). This suggests EXC-6 is not required to globally organize any of the three junction layers.

EXC-6-associated junctions “unzip” with oocyte entry.

Prior to ovulation, the spermatheca lumen is too small to accommodate an oocyte, and the smooth/continuous and the pleated septate junctions are folded. It is hypothesized that to permit oocyte entry, these folded junctions “unzip” to increase basal and luminal surface areas, respectively, while the adherens junctions maintain epithelium integrity (Figure 4 A; White, 1988; Creutz et al., 1996; Lints and Hall, 2009). Based on our determination that EXC-6 likely associates with the pleated septate junctions, we hypothesized EXC-6-decorated junctions might show evidence of this unzipping (Figure 4 A). Thus, we compared empty spermathecae of EXC-6::GFP-expressing worms with relatively rare spermathecae that were isolated with a resident oocyte/fertilized egg. We observed that in distended spermathecae containing an oocyte/egg, EXC-6::GFP loses its curly appearance in maximum intensity projections, suggesting that part of accommodation of oocyte entry is straightening of the spermatheca junctions (Figure 4 B). Additionally, the appearance of EXC-6-associated junctions in cross sections of spermathecae changed from orientations that were vertical or near-vertical relative to the lumen surface in empty spermathecae, to flattened, horizontal profiles relative to the lumen surface in distended spermathecae (Figure 4 B), suggesting EXC-6-associated junctions indeed unzip. Since such flattened junctions were not observed in empty spermathecae, we hypothesize that these junctions promptly re-zip on exit of the egg.

The EXC-6 C-terminal tail is necessary and sufficient for junction localization.

Many formins that associate with junctions use localization determinants in domains N-terminal to the FH1 and FH2 domains, but EXC-6 lacks such N-terminal domains (Figure 5 A). To test which domains mediate EXC-6 localization, we generated a series of EXC-6-coding cDNA constructs C-terminally tagged with GFP (Figure 5 A). These were cloned behind the *fln-1* gene promoter, which drives expression strongly in the spermatheca (Kovacevic and Cram, 2010), and these were microinjected into worms to produce heritable extrachromosomal arrays (ECAs). As ECAs can be inherited in a mosaic manner, *fln-1* promoter-driven *mCherry* was co-injected with all constructs to allow GFP-independent identification of transgenic spermathecae. Moreover, as different ECAs can result in differing levels of transgene expression (Mello et al., 1991), three lines for each construct were independently isolated. Finally, to avoid the possibility of localization due to dimerization with endogenous EXC-6, all injections were into *exc-6(gk386)* mutants, which exhibit no localized EXC-6 in the spermatheca (Figure 1 B).

Anti-GFP western blot analysis demonstrated expression levels varied widely across different constructs and different transgenic isolates, with the caveat that due to inconsistency of ECA inheritance, the fraction of animals that were transgenic varied from sample to sample. All lines expressed at least some fusion protein with mobility close to their predicted molecular weight (Supplementary Figure S2). Based on inspection of GFP fluorescence in mCherry-positive spermathecae in intact animals, almost all constructs exhibited some evidence of likely aggregation in the form of bright GFP puncta, but additional distinct localizations could also be observed. As expected, full length EXC-6::GFP predominantly localized to spermatheca junctions in the characteristic curly, ribbon-like pattern seen for endogenous EXC-6 (Figure 5 B). Junction localization was also observed in all EXC-6 constructs from which any single domain was removed (ΔH::GFP, ΔFH1::GFP, ΔID-FH2::GFP, and ΔFH2::GFP), with the exception of EXC-6 lacking the tail C-terminal to the FH2 domain (ΔC::GFP). Instead, ΔC::GFP fluorescence was diffuse in the cytoplasm (Figure 5 B).

In examining constructs composed of singular EXC-6 domains, we found the isolated helical N-terminus of EXC-6 tagged with GFP (H::GFP), and the tagged FH1 domain (FH1::GFP) also resulted in diffuse fluorescence in the cytoplasm, while the tagged FH2 domain (FH2::GFP), or the FH2 domain plus inter-FH1/FH2 sequence (ID-FH2::GFP), resulted in prominent nuclear fluorescence (Figure 5 B). Conversely, the isolated C-terminal tail of EXC-6 tagged with GFP (C::GFP) predominantly localized to junctions (Figure 5 B). All of these localizations were observed in > 90% of transgenic spermathecae in all three independently isolated transgenic lines for each construct. Thus the C-terminal tail is necessary and sufficient to localize EXC-6 to spermatheca junctions. The mechanism by which the C-terminal tail directs localization is unclear, but analysis using the Eukaryotic Linear Motif (ELM) resource (Dinkel et al., 2016) revealed 46 tail motifs, including two Wiskott-Aldrich syndrome protein homology-2 (WH2) domains predicted to bind actin monomers or filaments (Paunola et al., 2002; Carlier et al., 2013), multiple proline-rich motifs predicted to bind Src homology-3 (SH3) domains, and a putative microtubule end-

binding protein (EB)-binding SxIP motif (Honnappa et al., 2009) (Supplementary Figure S3).

exc-6(gk386) worms produce no detectable EXC-6.

Worms bearing *exc-6(gk386)* are defective for oocyte entry into the spermatheca during ovulation, but only partially so (Hegsted et al., 2016). Alternative possible explanations for this mild phenotype are that *exc-6(gk386)* worms retain some *exc-6* function, or that EXC-6 plays a non-essential role in this process. The allele *gk386* encodes a genomic deletion that eliminates part of the *exc-6* promoter, the first *exc-6* exon and intron, and part of the second exon, including sequences encoding the helical N-terminus and part of the FH1 domain (*C. elegans* Deletion Mutant Consortium et al., 2012; Mi-Mi et al., 2012). Due to the elimination of the promoter and start codon, *exc-6(gk386)* is predicted to completely eliminate the single known isoform of EXC-6, but it remained possible that alternative isoforms arise from cryptic promoters.

To test this, we probed worm extracts (normalized by whole protein content; Supplementary Figure S4) with a polyclonal antibody that was raised and affinity purified against the EXC-6 FH2 domain. Notably, the FH2-coding sequence is intact in *exc-6(gk386)* animals, being positioned downstream of the region deleted by *gk386* (Mi-Mi et al., 2012). To identify endogenous EXC-6 from among non-specific background signals, we compared extracts of control animals with those in which *exc-6* was knocked down through RNAi. We observed that *exc-6(RNAi)* correlated with loss of a single 105 kD band (Figure 6 A), which is only modestly larger than computationally predicted 94 kD for EXC-6. When *exc-6(gk386)* extracts were probed, the 105 kD band again was absent, and novel bands were not detected at lower or higher molecular weights (Figure 6 A), with two exceptions. One exception was the appearance of a 128 kD product in EXC-6::GFP-expressing transgenic worms, corresponding to an over-expressed tagged EXC-6. The second exception was a 100 kD band that appeared inconsistently across many different samples (for example, *asterisk* in lane 4 of Figure 6 A), but we determined that this band is a bacterial product derived from the *C. elegans* food source (Supplementary Figure S5). Thus, *exc-6(gk386)* produces no detectable protein, suggesting it is a null allele.

Consistent with this, we found *exc-6(gk386)* behaves as a recessive mutation with regard to ovulation (Figure 6 B). That is, normal ovulation events occurred in wild-type worms 87% of the time, a low value that is likely an artifact of treating animals with anesthetics, and mounting them for microscopy. Normal ovulations occurred in *exc-6(gk386)/(+)* heterozygous worms at a statistically indistinguishable frequency (85%, $p = 0.765$), whereas *exc-6(gk386)* homozygous worms showed a statistically significant decrease in normal ovulations to 63% ($p = 0.01$).

Expression of the EXC-6 C-terminal tail in the spermatheca exacerbates ovulation and transit defects.

To test whether expression of EXC-6 in the spermatheca improves ovulation in a background otherwise null for *exc-6* function, we examined ovulation in *exc-6(gk386)* mutants bearing ECAs with *fln-1* promoter-driven full-length EXC-6 (construct

EXC-6::GFP in Figure 5 A). As controls, we also examined *exc-6(gk386)* lines bearing ECAs with *fln-1p::mCherry* but no transgenic *exc-6*, as well as non-transgenic wild-type and *exc-6(gk386)* animals. In wild-type animals, oocyte maturation is normally quickly followed by ovulation (movement of the oocyte from the proximal gonad into the spermatheca), which is then followed by expulsion of the fertilized egg into the uterus (Figure 7, Supplementary Figure S6, Supplementary Video S1) (McCarter et al., 1999). The most prevalent defect observed in *exc-6(gk386)* animals was breakage of the oocyte during entry into the spermatheca, while rarer phenotypes included: breakage of the fertilized egg during exit from the spermatheca; failure of the oocyte to enter the spermatheca; or delay of exit of the fertilized egg from the spermatheca (Figure 7 C).

Wild-type worms ovulated normally 80% of the time under our observation conditions (again, likely an artifactual low percentage), while *exc-6(gk386)* worms ovulated normally only 54% of the time. As expected, *exc-6(gk386)* worms expressing only mCherry (*control strains #1–3*) had similar rates of ovulation failure as non-transgenic mutants (Figure 7 B). Full length EXC-6::GFP expressed from the *fln-1* promoter (+ *exc-6 #1–3*) had variable rates of normal ovulations. While none of these showed a statistically significant increase in normal ovulations from *exc-6(gk386)* controls, EXC-6::GFP-expressing strain #1 showed a trend toward normal ovulations that approached wild type (Figure 7 B). This differed from complete rescue by a genome-integrated *exc-6::gfp* transgene (Hegsted et al., 2016), but that rescuing construct was driven by the *exc-6* promoter, and retained *exc-6* introns and downstream sequences. It is possible that the *exc-6* cDNA used here is over- or under-expressed by the *fln-1* promoter or due to copy number. Also, excessive copies of the *fln-1* promoter, as would be caused by their presence in our ECAs, can perturb spermatheca function (Erin Cram, personal communication). Finally, potential mosaicism within the spermathecae could further impact rescue. Despite these caveats, the trend toward rescue seen in one strain suggests the possibility that expression of EXC-6 in the spermatheca is sufficient to improve ovulation.

Considering that the C-terminus of EXC-6 was sufficient for localizing GFP to the spermatheca junctions (Figure 5 B), we also tested whether C::GFP expression was sufficient to rescue ovulation in *exc-6(gk386)* worms. Strikingly, one C::GFP-expressing strain (#2) exhibited normal ovulation only 17% of the time, a statistically significant reduction from non-transgenic *exc-6(gk386)*, while the remaining two strains very modestly trended toward similar, but statistically insignificant reductions (Figure 7 B). Although western blot analysis suggests that the C::GFP-expressing strain #2 expresses the lowest level of fusion protein (Supplementary Figure S2), that interpretation is confounded by the variable heritability of ECAs, ensuring that samples analyzed for western blot are prepared from populations that are mixtures of transgenic and non-transgenic animals in varying proportions. By direct visual observation of transgenic animals, C::GFP-expressing strain #2 expresses noticeably higher levels of fusion protein in its spermatheca than the other two strains. Thus, the EXC-6 C-terminus is not sufficient for EXC-6 function, but in fact exacerbates ovulation. Moreover, the exacerbation of ovulation defects by C::GFP cannot be due to its interference with endogenous EXC-6, as it occurs in the *exc-6(gk386)* background which lacks any endogenous EXC-6 (Figure 6 A). Rather, these results suggest the EXC-6 tail interacts with additional factors critical for ovulation and spermatheca transit.

To determine whether enhanced ovulation defects in C::GFP-expressing worms correlate with F-actin disorganization, spermathecae were dissected from C::GFP-expressing animals (of strain #2), as well as EXC-6::GFP-expressing animals, and *exc-6(+)* and *exc-6(gk386)* controls, before staining with fluorescently labeled phalloidin to reveal F-actin (Supplementary Figure S7). The most notable cytoskeletal features of spermatheca cells are the prominent contractile F-actin-rich bundles associated with the basal surface. Consistent with our previous observations, cytoskeletal organization was virtually identical between wild type and *exc-6(gk386)* spermathecae (Hegsted et al., 2016; Supplementary Figure S7). Similar to what we observed in intact animals (Figure 5), EXC-6::GFP and C::GFP were primarily visible at spermatheca junctions in dissected gonads (Supplementary Figure S7). However, we could also observe in dissected gonads some association of both constructs with F-actin bundles, as well as some nuclear localization for C::GFP (Supplementary Figure S7). However, expression of neither construct resulted in notable disorganization of the contractile bundles (Supplementary Figure S7). Thus, the inhibitory effect of C::GFP is likely through a mechanism other than gross F-actin disorganization.

Identification of putative EXC-6 binding partners.

To identify proteins that might interact with EXC-6 and modulate its function or localization, we performed a yeast two-hybrid screen on a *C. elegans* cDNA library, using full-length EXC-6 as bait. From 2.3×10^6 transformants, seventeen clones representing eleven putative interactors were identified (Supplementary Table S1). Intriguing among these was JAC-1, a p120-catenin homolog that associates with many epithelial junctions (Pettitt et al., 2003), although this has not been examined in the spermatheca. Consistent our identification of an EB-binding SxIP motif in EXC-6, we also recovered multiple clones of the EB homologs EBP-1 and EBP-2, a finding of significance, as loss of EXC-6 from the excretory canal perturbs the directional growth of EBP-2-associated microtubules (Shaye and Greenwald, 2015). We also recovered an additional EBP-2-binding protein, the E3 ubiquitin ligase SIAH-1 (Li et al., 2004), suggesting the possibility that EXC-6, EBP-2, and SIAH-1 might form a ternary complex. Moreover, SIAH-1 was unique among yeast two-hybrid interactors for having been shown to be expressed in the spermatheca (McKay et al., 2003; Hunt-Newbury et al., 2007).

To test yeast two-hybrid interactors for functional interactions with EXC-6 in the spermathecae, we performed RNAi against a subset, and examined their effects on EXC-6::GFP localization, and on ovulation. For controls, we also targeted *exc-6* and *par-3* for RNAi. Verifying the efficacy of RNAi treatments, *par-3(RNAi)* resulted in nearly complete maternal effect embryonic lethality, while targeting of another putative interactor, *ifet-1*, caused a predicted similar but only partially penetrant lethality (Piano et al., 2002). Only *exc-6(RNAi)* resulted in loss of EXC-6::GFP from spermatheca junctions (Supplementary Figure S8), suggesting none of the tested candidates (nor PAR-3) individually is responsible for EXC-6 recruitment to junctions. RNAi-treated animals were also examined for an accumulation of endomitotic oocytes (Emo) phenotype, an effect observed in animals with severe ovulation defects (Iwasaki et al., 1996), As expected, the mild ovulation defects cause by *exc-6(RNAi)* did not result in an Emo phenotype (n = 30 animals from three replicate RNAi treatments), while *par-3(RNAi)* resulted in nearly 100%

Emo animals (n = 26 animals from three replicates), consistent with previous observations (Aono et al., 2004). The Emo phenotype was also evident in ~50% of *ifet-1(RNAi)* animals (n = 18 animals from three replicates). Whether this effect relates to EXC-6 is unclear, as *ifet-1* encodes a translational repressor, and no previous evidence has tied EXC-6 to protein synthesis. The remaining RNAi treatments showed no evidence of Emo phenotypes indicative of severe ovulation defects (n = 21 to 30 animals from three replicates per gene), but this result does not rule out the possibility of subtler ovulation defects as observed with loss of *exc-6* function.

Discussion:

The timely entry of oocytes into the spermatheca coincides with rapid expansion of the spermatheca lumen, an event expected to require remodeling of the junctions between spermatheca epithelial cells. In *Drosophila*, unzipping can occur along septate junctions during growth of glia cells (Babatz et al., 2018). The smooth/continuous septate junction layer of the *C. elegans* spermatheca junctions is analogous to the fly septate junctions in protein composition and in being positioned basal to a layer of adherens junctions (Lints and Hall, 2009; Pásti and Labouesse, 2014). Furthermore, the smooth/continuous septate junctions are contorted in the empty spermatheca, and are hypothesized to unzip during oocyte entry (White, 1988; Creutz et al., 1996; Lints and Hall, 2009). The spermatheca junctions also feature a unique layer apical to the adherens junctions. Called the pleated septate junction based on its appearance in electron micrographs (Lints and Hall, 2009), this apical layer is also contorted in the empty spermatheca, and is also predicted to unzip. We observe here that the formin EXC-6 is associated with a segment of the spermatheca junctions apical to the adherens junctions, likely the pleated septate junctions (Figure 2 and Figure 3). Moreover, this layer appears to “unzip” with oocyte entry, shifting from a highly contorted ribbon that is oriented along the apical/basal axis, to straight bands that are flattened in the plane of the apical surface (Figure 4). This is strongly reminiscent of the myosin phosphatase regulatory subunit MEL-11, which has also been observed associated with the apical segment of spermatheca junctions that are highly contorted in the empty spermatheca, but straighten during oocyte entry (Simske, 2013).

In the absence of EXC-6, entry of the oocyte into the spermatheca is slowed, often leading to rupture of oocytes as the spermatheca constricts before entry is complete (Hegsted et al., 2016). How EXC-6 affects this process is unclear. We have observed that EXC-6 potently stimulates the assembly of actin filaments *in vitro* similar to other formins (data not shown), but loss of EXC-6 has no apparent effect on the organization of the prominent F-actin bundles that directly mediate contraction of the spermatheca (Hegsted et al., 2016). One plausible alternative suggestion is that EXC-6 assists spermatheca expansions during oocyte entry by facilitating pleated septate junction unzipping, perhaps by remodeling actin filaments that underlie the junctions (Hegsted et al., 2016). The additional presence at these junctions of apical PAR proteins PAR-3 and PAR-6, as well as MEL-11, suggests actin modulatory activity of EXC-6 might coordinate with myosin inhibition by MEL-11, and scaffolding functions of the PAR proteins.

The C-terminal tail of EXC-6 is necessary and sufficient to recruit the formin to junctions (Figure 5). Interestingly, the two closest human homologs of EXC-6 can also localize via C-terminal tail motifs: FHDC1/INF1 associates with Golgi-associated microtubules through a C-terminal microtubule-binding domain, and an isoform of INF2 associates with the endoplasmic reticulum through prenylation of a C-terminal CAAX-box (Young et al., 2008; Chhabra et al., 2009; Copeland et al., 2016). EXC-6 lacks a CAAX box and shows no homology to the FHDC1/INF1 microtubule-binding domain, but analysis of the EXC-6 tail identified a series of motifs predicted to interact with additional cytoskeletal proteins, including two actin-binding WH2 domains, a multitude of predicted SH3-binding motifs, and an SxIP motif expected to bind EB proteins (Honnappa et al., 2009) (Supplementary Figure S3). Interestingly, in a yeast two-hybrid assay, EXC-6 interacts with two EB homologs EBP-1 and EBP-2, and with the EBP-2-binding protein, SIAH-1 (SupplementaryTable S1). RNAi-mediated knockdown of these showed no effect on ovulation or EXC-6 localization in the spermatheca (Supplementary Figure S8), but these interactions could be of significance in the excretory canal, where EXC-6 localizes along microtubules, and its absence perturbs the organization of EBP-2-bound microtubules (Shaye and Greenwald, 2015).

Interestingly, not only is EXC-6 C-terminal tail sufficient for localization to the spermatheca junctions, its expression enhanced the frequency of ovulation defects in *exc-6(gk386)* animals (Figure 7), indicating interaction with the EXC-6 tail can alter the function of other components important for ovulation. Notably, this negative effect on ovulation cannot be due to the tail blocking full-length EXC-6 from interacting with other ovulation components, as this effect occurs in *exc-6(gk386)* animals that produce no detectable EXC-6 (Figure 6 and Figure 7). Nor is this effect likely to be due to interference with a homologous formin, as the tail sequence of even the next closest formin homolog, INFT-2, bears no detectable similarity to that of EXC-6. It will be of interest to identify functional binding partners for the EXC-6 tail, and to determine how binding to the tail alone or to full-length EXC-6 alters their function.

There are intriguing parallels between EXC-6 in the worm spermatheca, and human INF2 in kidney podocytes. Podocytes are unique epithelial cells that line the outer surfaces of glomerular capillaries with numerous interdigitated foot processes that make specialized cell-cell junctions, called slit diaphragms. Notably, podocytes can undergo a dramatic morphological change called foot process effacement (FPE), in which the narrow foot processes become broad and flat. FPE can occur within minutes, and is considered a protective response to preserve podocyte attachment under conditions of increased mechanical stress, such as during chronic kidney disease (reviewed in Kriz and Lemley, 2015). Notably, a number of *INF2* mutations in humans can cause the kidney disease focal segmental glomerulosclerosis accompanied by FPE (Brown et al., 2010; Boyer et al., 2011), and a mouse *INF2* mutant model shows an inability to reverse the transient FPE that occurs after induced acute kidney injury (Subramanian et al., 2016). INF2 is expressed in podocytes, and localizes in part to slit diaphragms, suggesting the formin might contribute directly to the reversible plasticity of these junctions. But how INF2 functions in podocytes, and the effects of many *INF2* mutations on INF2 protein function, remain unclear. An exciting possibility is that the resemblance of INF2 to EXC-6 at spermatheca junctions is

more than superficial, but reflects a deeper conserved function for these related formins. In such a case, ovulation in the *exc-6(gk386)* worm might serve as a simple, genetically-tractable model for testing whether novel *INF2* mutations identified in patients have functional consequences for junctional plasticity.

Materials and Methods:

Plasmids

All plasmids and primers used in this study are listed in Supplementary Table S2 and Supplementary Table S3, respectively. To drive expression of full-length EXC-6 tagged with GFP in the spermatheca, *exc-6* cDNA (Mi-Mi et al., 2012) was amplified with 5' *XbaI* site and 3' linker (encoding Gly-Ala-Gly-Ala-Gly) sequences, and *linker::gfp* was amplified from pRS315-*exc-6::gfp* (Hegsted et al., 2016) with a 3' *XmaI* site. These were joined by fusion PCR and TOPO-TA cloned into pCR4BTOPO to produce pAH1 (pCR4BTOPO *exc-6::gfp*). Plasmid pAH2 was constructed by subcloning *XbaI exc-6::gfp XmaI* between the *fln-1* promoter and the *fln-1* 3' UTR in pUN107, a gift from Erin Cram (Northwestern University, Boston, MA). The *fln-1* promoter expresses in cells of the spermatheca, proximal gonad sheath, uterus and elsewhere (Kovacevic and Cram, 2010), but we observed expression of GFP only in the spermatheca.

To produce a co-reporter for expression in spermatheca cells, pAH24 was created by amplifying *mCherry* from pCJF104 with 5' *XbaI* and 3' *XmaI* sites before cloning between the *fln-1* promoter and the *fln-1* 3' UTR of pUN107.

To test for the domain requirements for EXC-6 localization in the spermatheca, cDNAs encoding the following regions of EXC-6 were individually joined by fusion PCR to *linker::gfp*: helical region (H; encoded by *exc-6* cDNA base pairs 1–198); FH1 domain (base pairs 199–306); FH2 domain (base pairs 385–1617); interdomain region between FH1 and FH2 (ID) plus the FH2 domain (ID-FH2; base pairs 307–1617); and C-terminal tail (C; base pairs 1618–2532). *Domain::gfp* constructs were subcloned between the *fln-1* promoter and *fln-1* 3'UTR to produce the plasmids listed in Supplementary Table S2.

To make *exc-6::gfp* constructs with specific domains deleted (ΔH, ΔFH1, ΔFH2, ΔID-FH2, or ΔC), regions 5' and 3' to the deletion were amplified from pAH1. The 5' portion was engineered with a 5' *XbaI* site and a 3' overlap sequence. The 3' portion was engineered with a 5' overlap sequence and a 3' *XmaI* site. These were joined by fusion PCR and subcloned as above.

The bait construct plasmid pAH25 for yeast two-hybrid screening was produced by amplification of full length *exc-6* cDNA with flanking *KpnI* and *SacII* restriction sites, followed by cloning into the bait plasmid pLexA-C (DualSystemsBiotech yeast two-hybrid kit; Schlieren, Switzerland).

For RNAi studies, we used previously generated double stranded RNA expression vector L4440 (Timmons and Fire, 1998), L4440-*exc-6* (Mi-Mi et al., 2012), and L4440-*par-3* (a gift from K. J. Kemphues, Cornell University, Ithaca NY; Aono et al., 2004). To knock down

putative EXC-6-binding candidates isolated in our yeast two-hybrid screen, 200–300 bp of cDNA of each candidate was amplified by PCR on recovered yeast two-hybrid plasmids, and cloned into *SmaI*-linearized L4440 by In-Fusion Cloning using CloneAmp HiFi PCR Premix (Takara Bio USA Incorporated, Mountain View, CA).

The complete sequences for all cloned PCR products were verified by sequence analysis.

Worm strains and growth conditions

Worms were grown under standard conditions at 20°C (Brenner, 1974). For complete genotypes of strains used in this study, see Supplementary Table S4. Worm strains N2, FT17, FT63, FT250, HR596, JJ1440, and ST65 were obtained from the *Caenorhabditis* Genetic Center (University of Minnesota, Minneapolis, MN). SU131 was a gift from J. Hardin (University of Wisconsin-Madison, Madison, WI; Simske et al., 2003).

RNAi-mediated knockdowns were performed by the standard feeding technique (Wang and Barr, 2005). Briefly, *Escherichia coli* HT115 was transformed with L4440 negative control or appropriate knockdown vector, and grown overnight at 37°C in 2xYT medium with 12.5 μg/ml tetracycline and 100 μg/ml ampicillin. Cultures were then diluted 1:100 in 2xYT, grown 3 hr at 37°C, and then induced with 0.4 mM IPTG for further 3 hr at 37°C. Induced cultures were concentrated five-fold and seeded onto plates. For knockdown of genes predicted to not be essential (*exc-6*, *ebp-1*, *ebp-2*, *C50F4.1*, *siah-1*, *jac-1*) (Kamath et al., 2003; Raul et al., 2004; Skop et al., 2004; Fernandez et al., 2005; Sönnichsen et al., 2005), worms were continuously treated for RNAi for a minimum of three generations. For knockdowns predicted to be lethal or partially lethal (*par-3*, *ifet-1*) (Kamath et al., 2001; Piano et al., 2002), L1 worms were plated onto RNAi plates and inspected as adults after 2 days (to inspect spermathecae junctions) or 3 days (to examine for endomitotic oocytes) at 20°C.

To make transgenic worms expressing full length or partial *fln-1p::exc-6::linker::gfp* constructs, XA8004 *exc-6(gk386)* hermaphrodites were injected with 25 ng/μl of the relevant *exc-6* construct plasmid, plus mCherry-expressing co-injection markers (10 ng/μl pAH24, 10 ng/μl pGH8 and 2.5 ng/μl pCFJ90) (Frøkjaer-Jensen et al., 2008) and 75 ng/μl of pRS315 (Sikorski and Hieter, 1989).

Microscopy and image analysis of live animals

To image spermathecae in live animals, adult hermaphrodite worms were paralyzed in M9 containing 0.1% tricaine (Acros Organics, Geel, Belgium) and 0.01% levamisole (Acros Organics, Geel, Belgium), and live mounted onto a 2% agarose pad. Epifluorescence and differential interference contrast (DIC) images were obtained using an Eclipse 90i research upright microscope (Nikon, Tokyo, Japan) at room temperature using a CFI Plan Apochromat 403/NA 1.0 oil immersion objective, with a Cool-SNAP HA2 digital monochrome charge-coupled device camera (Photometrics, Tucson, AZ) driven by NIS-Elements AR acquisition and analysis software (version 3.1; Nikon). Ovulation movies were acquired using DIC microscopy as previously described (Hegsted et al., 2016). Spermathecae expressing mCherry were scored for localization of GFP as junctional, nuclear, or cytoplasmic. For spermathecae selected for imaging, Z-stacks were collected at

2.5 μm intervals before deconvolution in NIS-Elements using AutoQuant Blind Deconvolution, with 17 iterations and medium noise level. Spermathecae outlines indicted in Figure 5 B were determined using mCherry fluorescence.

Microscopy and image analysis of fixed samples

Primary and secondary antibodies used for immunofluorescence microscopy were pre-cleared to remove non-specific staining. Briefly, to preclear anti-EXC-6 (DPMSP5; Mi-Mi et al., 2012), 15–30 worms treated for *exc-6(RNAi)* were paralyzed briefly in 0.2 mM levamisole, and dissected in PBS on poly-L-lysine-coated slides to expose the gonad, before 5 min fixation in −20μC MeOH and two brief washes in PBST (1x PBS; 0.1% Tween-20). Samples were then incubated 1 hr with PBST containing 0.1% goat serum with 1:10 dilution of DPMSP5. The antibody solution was recovered from slides and diluted for use as primary antibody for immunofluorescence microscopy. To pre-clear Texas Red-labeled goat anti-rabbit (Rockland Immunochemicals, Pottstown, PA), wild-type worms were similarly paralyzed, dissected, and fixed, before being blocked 1 hr in PBST containing 1% goat serum, washed twice briefly with PBST, and incubated overnight in PBST containing 0.1% goat serum and 1:1000 dilution Texas Red-labeled goat anti-rabbit. This solution was recovered from slides and diluted for use as secondary antibody for immunofluorescence microscopy.

To immunostain extruded worm gonads, worms were paralyzed, dissected, and fixed as above, before being blocked 1 hr in PBST containing 1% goat serum and then washed twice briefly in PBST. Samples were then incubated overnight in primary solution (pre-cleared DPMPS5 diluted to a final 1:100 in PBST + 0.1% goat serum). The following day, samples were washed twice briefly with PBST, incubated 2 hr in secondary solution (pre-cleared Texas Red-labeled goat anti-rabbit diluted to a final 1:2000 in PBST + 0.1% goat serum), and then washed twice briefly in PBST. Stained samples were covered with VECTASHIELD mounting medium (Vector Laboratories, Burlingame, CA). To stain extruded worm gonads with fluorescent phalloidin to visualize F-actin, or to stain whole worms with 4’,6-diamidino-2-phenylindole to visualize DNA for identification of endomitotic oocyts, worms were treated as described previously (Hegsted et al., 2016).

Confocal images were obtained on an SP5 laser-scanning confocal microscope (Leica, Wetzlar, Germany) driven by LAS AF Software (version 2.2.0, build 4758; Leica), and using an HCX Plan Apochromat 63x/NA 1.4 oil lambda objective. Confocal stacks were analyzed in IMARIS (Bitplane, Belfast, UK) using the section tool to create XY maximum intensity projections, and XZ or YZ cross-sections. All images were edited linearly and colored in Photoshop CS4 (Adobe, San Jose, CA).

Line scans were made in ImageJ (version 2.0.0-rc-65/1.51u; Schneider et al., 2012) using a one pixel-wide line and the “plot profile” function. To determine the distance between peak intensities of GFP and EXC-6 immunostain, lines were drawn through every GFP puncta towards the spermatheca lumen in XZ images in confocal cross-sections. The position of the maximal peak intensity for each EXC-6 immunostained puncta was set to zero, and the distance to the peak maximal intensity of GFP fluorescence was measured. Positive values

reflect an apical localization of GFP relative to EXC-6, while negative values reflect a basal localization.

Western blot analysis

Worm lysates were obtained by suspending mixed-stage populations of worms in 2x reducing sample buffer, boiling for 3 min, homogenizing worms with a tissue homogenizer (VWR International), and boiling 3 min again. HT115 *E. coli* extracts were obtained by washing plates lacking worms with M9, as would be done for collecting worms. Samples were then centrifuged at low speed (1000 rpm) for 1 min, as would be done to collect worms, or at maximum speed in a microfuge for 1 min, to concentrate bacteria. HT115 samples were then treated identically as above for worm lysates. Genomic DNA in all lysates was sheared by eight passages through an insulin syringe. Samples were normalized by comparing Coomassie brilliant blue stain of total lanes after SDS-PAGE (Bio-Rad, Hercules, CA).

For western blot analysis, proteins were resolved by SDS-PAGE and transferred to PVDF (Millipore, Burlington, MA) or nitrocellulose (Bio-Rad, Hercules, CA) for immunoblotting. After blocking in 10% milk, blots were incubated with primary antibody diluted 1:100 (anti-EXC-6 DPMSP8; Mi-Mi et al., 2012) or 1:1000 (anti-GFP GF23R; Invitrogen, Carlsbad, CA) in TBST (50 mM Tris-HCl, pH 8.3; 150 mM NaCl; 0.3% Tween 20) containing 1% milk. Primary incubations were for 3 hr (DPMSP8) or 1 hr (GF28R) at room temperature. Blots were incubated in goat anti-rabbit-HRP or goat anti-mouse-HRP secondary antibodies diluted 1:3000 in TBST containing 1% milk for 1 hr at room temperature. Images were acquired using a Bio-Rad ChemiDoc MP imager (Hercules, CA), and processed with Image Lab and Photoshop CS4.

A note on anti-EXC-6, the affinity purified antibodies DPMSP5 and DPMSP8 were isolated from different rabbits. By western blot, both recognize identical bands, but DPMSP8 provides a significantly stronger western signal, and thus was used here for that purpose. However, only DPMSP5 was found to be suitable for immunofluorescence microscopy, with DPMSP8 resulting in non-specific stain only.

Yeast two-hybrid screen

The yeast two-hybrid screen was performed using the DualSystemsBiotech kit (Schlieren, Switzerland), as per instructions. Briefly, the bait construct pAH25 encoding full-length *exc-6* cDNA was screened for interactions in NMY51 yeast against a *C. elegans* adult cDNA library (DualSystemsBiotech). Prey plasmids were isolated from clones able to grow under selective conditions (media lacking histidine and containing 1 mM 3-amino-1,2,4-triazole), and retransformed to NMY51 to confirm their EXC-6-dependence before being subject to sequence analysis for identification.

Ethical considerations

This study did not involve the use of human subjects or vertebrate animals. *C. elegans* is an invertebrate model that is not covered by the guidelines of National Institutes of Health definition of Laboratory Animal, and is not subject to regulation by the SUNY Upstate

Medical University Institutional Animal Care and Use Committee. All protocols and procedures were approved by the SUNY Upstate Medical University Institutional Biosafety Committee, and followed NIH Guidelines for Research Involving Recombinant DNA Molecules.

Data availability statement

The data supporting the findings of this study are available from the corresponding author upon reasonable request.

Statistical analysis

Bar graphs were made in Excel:mac (version 14.7.2 and 14.7.7; Microsoft Corporation, Redmond, WA) and line graphs were made in KaleidaGraph (version 4.5.2; Synergy Software, Reading, PA). Measurements of distance between maximal GFP fluorescence and maximal EXC-6 immunostain along spermatheca junctions were subject to analysis of variation, with Tukey-Kramer post-hoc testing. Differences for which $p < 0.05$ were considered statistically significant. Quantitative ovulation data were analyzed using a chi-squared test of independence, with post-hoc testing using a Bonferroni corrected p-value = α / # of tests, where $\alpha = 0.05$. See Supplementary Table S5 for details.

Supplementary Material

Refer to Web version on PubMed Central for supplementary material.

Acknowledgments:

Thanks to E. Cram, K. J. Kemphues, and A. Fire Laboratory for plasmids, J. Hardin for worm strains, the Handbook of Biological Statistics, WormBase, and WormAtlas. Many strains were obtained from the CGC, which is funded by NIH Office of Research Infrastructure Programs (P40 OD010440). This work was supported by NIAMS of the NIH under Award Number R01AR064760 to D. P.

References:

Achilleos A , Wehman AM , Nance J (2010). PAR-3 mediates the initial clustering and apical localization of junction and polarity proteins during *C. elegans* intestinal epithelial cell polarization. Development, 137, 1833–1842. [PubMed: 20431121]

Anderson DC , Gill JS , Cinalli RM , Nance J (2008). Polarization of the *C. elegans* embryo by RhoGAP-mediated exclusion of PAR-6 from cell contacts. Science, 320, 1771–1774. [PubMed: 18583611]

Aono S , Legouis R , Hoose WA , Kemphues KJ (2004). PAR-3 is required for epithelial cell polarity in the distal spermatheca of *C. elegans*. Development, 131, 2865–2874. [PubMed: 15151982]

Brenner S (1974). The genetics of *Caenorhabditis elegans*. Genetics, 77, 71–94. [PubMed: 4366476]

Boyer O , Nevo F , Plaisier E , et al. (2011). INF2 mutations in Charcot-Marie-Tooth disease with glomerulopathy. N Engl J Med, 365, 2377–2388. [PubMed: 22187985]

Brown EJ , Schlöndorff JS , Becker DJ , Tsukaguchi H , Tonna SJ , Uscinski AL , Higgs HN , Henderson JM , Pollak MR (2010). Mutations in the formin gene INF2 cause focal segmental glomerulosclerosis. Nat Genet, 42, 72–76. [PubMed: 20023659]

Breitsprecher D , & Goode BL (2013). Formins at a glance. J Cell Sci, 126, 1–7. [PubMed: 23516326]

C. elegans Deletion Mutant Consortium, Barstead R , Moulder G , et al. (2012). Large-scale screening for targeted knockouts in the Caenorhabditis elegans genome. G3 (Bethesda), 2, 1415–1425. [PubMed: 23173093]

Carlier MF , Pernier J , Avvaru BS (2013). Control of actin filament dynamics at barbed ends by WH domains: from capping to permissive and processive assembly. Cytoskeleton (Hoboken), 70, 540–549. [PubMed: 23843333]

Chhabra ES, Ramabhadran V , Gerber SA , Higgs HN (2009). INF2 is an endoplasmic reticulum-associated formin protein. J Cell Sci, 122, 1430–1440. [PubMed: 19366733]

Copeland SJ , Thurston SF , Copeland JW (2016). Actin- and microtubule-dependent regulation of Golgi morphology by FHDC1. Mol Biol Cell, 27, 260–276. [PubMed: 26564798]

Costa M , Raich W , Agbunag C , Leung B , Hardin J , Priess JR (1998). A putative catenin-cadherin system mediates morphogenesis of the *Caenorhabditis elegans* embryo. J Cell Biol, 141, 297–308. [PubMed: 9531567]

Creutz CE , Snyder SL , Daigle SN , Redick J (1996). Identification, localization, and functional implications of an abundant nematode annexin. J Cell Biol, 132, 1079–1092. [PubMed: 8601586]

Dinkel H , Van Roey K , Michael S , et al. (2016). ELM 2016--data update and new functionality of the eukaryotic linear motif resource. Nucleic Acids Res, 44, D294–300. [PubMed: 26615199]

Fernandez AG , Gunsalus KC , Huang J , et al. (2005). New genes with roles in the *C. elegans* embryo revealed using RNAi of ovary-enriched ORFeome clones. Genomes Res, 15, 250–259.

Frøkjaer-Jensen C , Davis MW , Hopkins CE , Newman BJ , Thummel JM , Olesen SP , Grunnet M , Jorgensen EM (2008). Single-copy insertion of transgenes in *Caenorhabditis elegans*. Nat Genet, 40, 1375–1383. [PubMed: 18953339]

Goode BL , & Eck MJ (2007). Mechanism and function of formins in the control of actin assembly. Annu Rev Biochem, 76, 593–627. [PubMed: 17373907]

Grikscheit K , & Grosse R (2016). Formins at the Junction. Trends Biochem Sci, 41, 148–159. [PubMed: 26732401]

Hegsted A , Wright FA , Votra S , Pruyne D (2016). INF2- and FHOD-related formins promote ovulation in the somatic gonad of *C. elegans*. Cytoskeleton (Hoboken), 73, 712–728. [PubMed: 27770600]

Hegsted A , Yingling CV , Pruyne D (2017). Inverted formins: A subfamily of atypical formins. Cytoskeleton (Hoboken), 74, 405–419. [PubMed: 28921928]

Honnappa S , Gouveia SM , Weisbrich A , et al. (2009). An EB1-binding motif acts as a microtubule tip localization signal. Cell, 138, 366–376. [PubMed: 19632184]

Hunt-Newbury R , Viveiros R , Johnsen R , et al. (2007). High-throughput in vivo analysis of gene expression in *Caenorhabditis elegans*. PLoS Biol, 5, e237 10.1371/journal.pbio.0050237 [PubMed: 17850180]

Iwasaki K , McCarter J , Francis R , Schedl T (1996). emo-1, a *Caenorhabditis elegans* Sec61p gamma homologue, is required for oocyte development and ovulation. J Cell Biol, 134, 699–714. [PubMed: 8707849]

Jefferson JA , & Shankland SJ (2014). The pathogenesis of focal segmental glomerulosclerosis. Adv Chronic Kidney Dis, 21, 408–416. [PubMed: 25168829]

Kamath RS , Fraser AG , Dong Y , et al. (2003). Systematic functional analysis of the *Caenorhabditis elegans* genome using RNAi. Nature, 421, 231–237. [PubMed: 12529635]

Kamath RS , Martinez-Campos M , Zipperlen P , Fraser AG , Ahringer J (2001). Effectiveness of specific RNA-mediated interference through ingested double-stranded RNA in *Caenorhabditis elegans*. Genome Biol, 2, RESEARCH0002. 10.1186/gb-2000-2-1-research0002

Köppen M , Simske JS , Sims PA , Firestein BL , Hall DH , Radice AD , Rongo C , Hardin JD (2001). Cooperative regulation of AJM-1 controls junctional integrity in *Caenorhabditis elegans* epithelia. Nat Cell Biol, 3, 983–991. [PubMed: 11715019]

Kovacevic I , & Cram EJ (2010). FLN-1/filamin is required for maintenance of actin and exit of fertilized oocytes from the spermatheca in *C. elegans*. Dev Biol, 347, 247–257. [PubMed: 20707996]

Kriz W , & Lemley KV (2015). A potential role for mechanical forces in the detachment of podocytes and the progression of CKD. J Am Soc Nephrol, 26, 258–269. [PubMed: 25060060]

Li S , Bertin CM , Ge H , et al. (2004). A map of the interactome network of the metazoan *C. elegans*. Science, 303, 540–543. [PubMed: 14704431]

Lints R , & Hall DH (2009). Reproductive system, somatic gonad In: WormAtlas: Herndon LA-ed. 10.3908/wormatlas.1.22

McCarter J , Bartlett B , Dang T , Schedl T (1999). On the control of oocyte meiotic maturation and ovulation in *Caenorhabditis elegans*. Dev Biol, 205, 111–128. [PubMed: 9882501]

McKay SJ , Johnsen R , Khattra J , et al. (2003). Gene expression profiling of cells, tissues, and developmental stages of the nematode *C. elegans*. Cold Spring Harb Symp Quant Biol, 68, 159–69. [PubMed: 15338614]

McMahon L , Legouis R , Vonesch JL , Labouesse M (2001). Assembly of *C. elegans* apical junctions involves positioning and compaction by LET-413 and protein aggregation by the MAGUK protein DLG-1. J Cell Sci, 114, 2265–2277. [PubMed: 11493666]

Mello CC , Kramer JM , Stinchcomb D , Ambros V (1991). Efficient gene transfer in *C. elegans*: extrachromosomal maintenance and integration of transforming sequences. EMBO J, 10, 3959–3970. [PubMed: 1935914]

Mi-Mi L , Votra S , Kemphues K , Bretscher A , Pruyne D (2012). Z-line formins promote contractile lattice growth and maintenance in striated muscles of *C. elegans*. J Cell Biol, 198, 87–102. [PubMed: 22753896]

Nance J , Munro EM , Priess JR (2003). *C. elegans* PAR-3 and PAR-6 are required for apicobasal asymmetries associated with cell adhesion and gastrulation. Development, 130, 5339–5350. [PubMed: 13129846]

Pásti G , & Labouesse M (2014). Epithelial junctions, cytoskeleton, and polarity. In Wormbook: The C. elegans community-ed 10.1895/wormbook.1.56.2

Paunola E , Mattila PK , Lappalainen P (2002). WH2 domain: a small, versatile adapter for actin monomers. FEBS Lett, 513, 92–97. [PubMed: 11911886]

Pettitt J , Cox EA , Broadbent ID , Flett A , Hardin J (2003). The *Caenorhabditis elegans* p120 catenin homolog, JAC-1, modulates cadherin-catenin function during epidermal morphogenesis. J Cell Biol, 162, 15–22. [PubMed: 12847081]

Piano F , Schetter AJ , Morton DG , Gunsalus KC , Reinke V , Kim SK , Kemphues KJ (2002). Gene clustering based on RNAi phenotypes of ovary-enriched genes in *C. elegans*. Curr Biol, 12, 1959–1964. [PubMed: 12445391]

Pruyne D (2016). Revisiting the phylogeny of the animal formins: two new subtypes, relationships with Multiple Wing Hairs proteins, and a lost human formin. PLoS One, 11, e0164067. [PubMed: 27695129]

Raul JF , Ceron J , Koreth J , Hao T , Nicot AS , Hirozane-Kishikawa T , Vandenhaute J , Orkin SH , Hill DE , van den Heuvel S , Vidal M (2004). Toward improving *Caenorhabditis elegans* phenome mapping with an ORFeome-based RNAi library. Genome Res, 14, 2162–2168. [PubMed: 15489339]

Schneider CA , Rasband WA , Eliceiri WW (2012). NIH Image to ImageJ: 25 years of image analysis. Nat Methods, 9, 671–675. [PubMed: 22930834]

Shaye DD , & Greenwald I (2015). The disease-associated formin INF2/EXC-6 organizes lumen and cell outgrowth during tubulogenesis by regulating F-actin and microtubule cytoskeletons. Dev Cell, 32, 743–755. [PubMed: 25771894]

Sikorski RS , & Hieter P (1989). A system of shuttle vectors and yeast host strains designed for efficient manipulation of DNA in *Saccharomyces cerevisiae*. Genetics, 122, 19–27. [PubMed: 2659436]

Simske JS (2013). Claudins reign: The claudin/EMP/PMP22/γ channel protein family in *C. elegans*. Tissue Barriers, 1, e25502. [PubMed: 24665403]

Simske JS , Köppen M , Sims P , Hodgkin J , Yonkof A , Hardin J (2003). The cell junction protein VAB-9 regulates adhesion and epidermal morphology in *C. elegans*. Nat Cell Biol, 5, 619–625. [PubMed: 12819787]

Skop AR , Liu H , Yates J 3rd. , Meyer BJ , Heald R. (2004). Dissection of the mammalian midbody proteome reveals conserved cytokinesis mechanisms. Science, 305, 61–66. [PubMed: 15166316]

Sönnichsen B , Koski LB , Walsh A , et al. (2005). Full-genome RNAi profiling of early embryogenesis in *Caenorhabditis elegans*. Nature, 434, 462–469. [PubMed: 15791247]

Subramanian B , Sun H , Yan P , Charoonratana VT , Higgs HN , Wang F , Lai KV , Valenzuela DM , Brown EJ , Schlöndorff JS , Pollak MR (2016). Mice with mutant Inf2 show impaired podocyte and slit diaphragm integrity in response to protamine induced kidney injury. Kidney Int, 90, 363–372. [PubMed: 27350175]

Timmons L , & Fire A (1998). Specific interference by ingested dsRNA. Nature, 395, 854. [PubMed: 9804418]

Wang J , & Barr MM (2005). RNA interference in *Caenorhabditis elegans*. Methods Enzymol, 392, 36–55. [PubMed: 15644174]

Ward S , & Carrel JS (1979). Fertilization and sperm competition in the nematode *Caenorhabditis elegans*. Dev Biol, 73, 304–321. [PubMed: 499670]

White J (1988). The Anatomy. In: The Nematode Caenorhabditis elegans. Cold Spring Harbor Laboratory Press, Cold Spring Harbor, NY: Wood WB-ed.

Wissmann A , Ingles J , Mains PE (1999). The *Caenorhabditis elegans mel-11* myosin phosphatase regulatory subunit affects tissue contraction in the somatic gonad and the embryonic epidermis and genetically interacts with the Rac signaling pathway. Dev Biol, 209, 111–127. [PubMed: 10208747]

Young KG , Thurston SF , Copeland S , Smallwood C , Copeland JW (2008). INF1 is a novel microtubule-associated formin. Mol Biol Cell, 19, 5168–5180. [PubMed: 18815276]

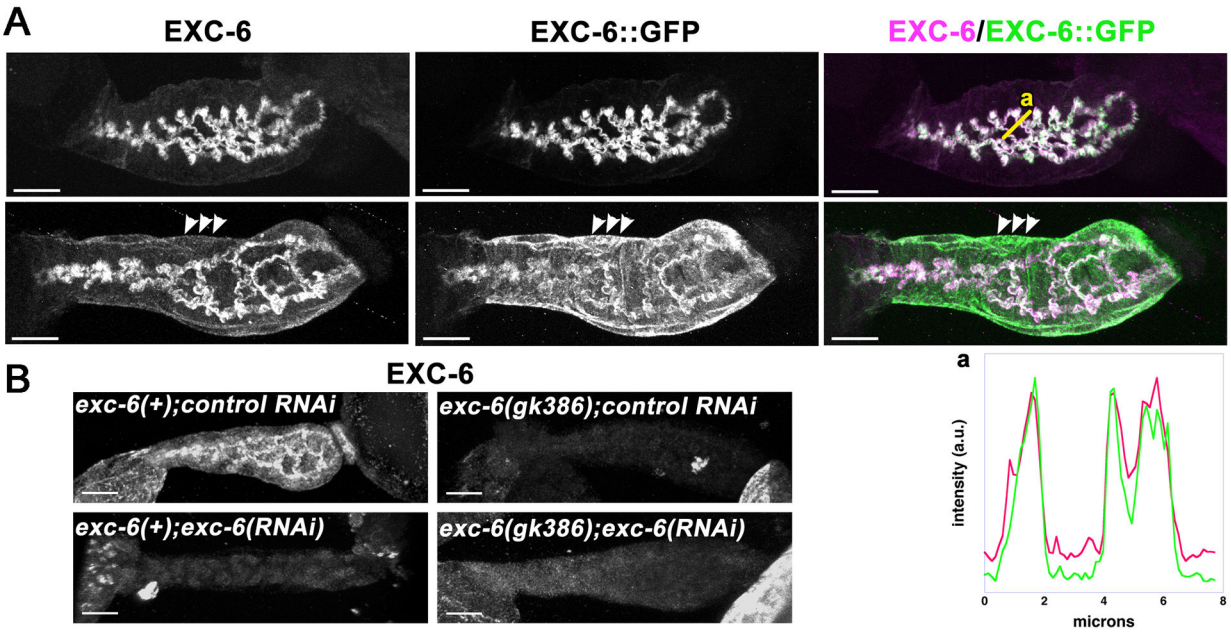

Figure 1.

Endogenous EXC-6 localizes to cell-cell junctions in the spermatheca. (A) Confocal micrographs of spermathecae dissected from EXC-6::GFP-expressing worms were stained with anti-EXC-6. *Top* images show a spermatheca with typical junction localization, while *bottom* images show a spermatheca with GFP/EXC-6-positive junctions and less common basal fibers (*arrowheads*). Graphed fluorescence intensities for anti-EXC-6 (*magenta*) and EXC-6::GFP (*green*) along line *a* show strong colocalization at junctions. (B) Confocal micrographs of dissected spermathecae from non-transgenic worms stained with anti-EXC-6 show endogenous EXC-6 localizes predominantly to junctions, but is lost from worms treated for *exc-6(RNAi)* or bearing *exc-6(gk386)*. Scale bars, 10 μm.

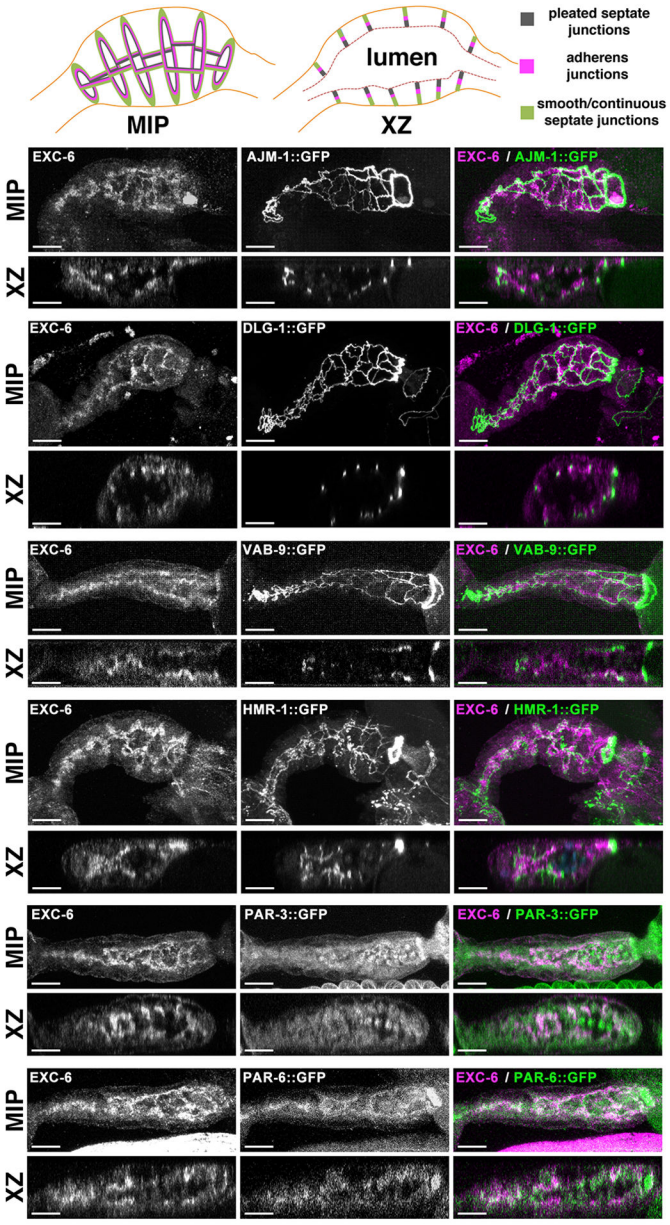

Figure 2.

EXC-6 localization relative to known junction markers. Spermathecae from worms expressing junction proteins fused to GFP were dissected and immunostained for EXC-6. Simplified spermathecae models (*top*) show idealized expected appearance of pleated septate, adherens, and smooth/continuous septate junction markers relative to basal (*solid line*) and apical (*dotted line*) surfaces of the spermatheca epithelium in maximum intensity projections (*MIP*) and longitudinal sections (*XZ*). Markers examined include smooth/continuous septate junction proteins AJM-1::GFP and DLG-1::GFP, adherens junction proteins VAB-9::GFP and HMR-1::GFP, and apically-positioned proteins PAR-3::GFP and PAR-6::GFP. In favorable sections, EXC-6 often appears apical to smooth/continuous septate junctions and adherens junctions, but overlaps or is slightly basal to apical markers,

suggesting EXC-6 likely associates with the pleated septate junctions that are positioned apical to the adherens junctions. Scale bars, 10 μm.

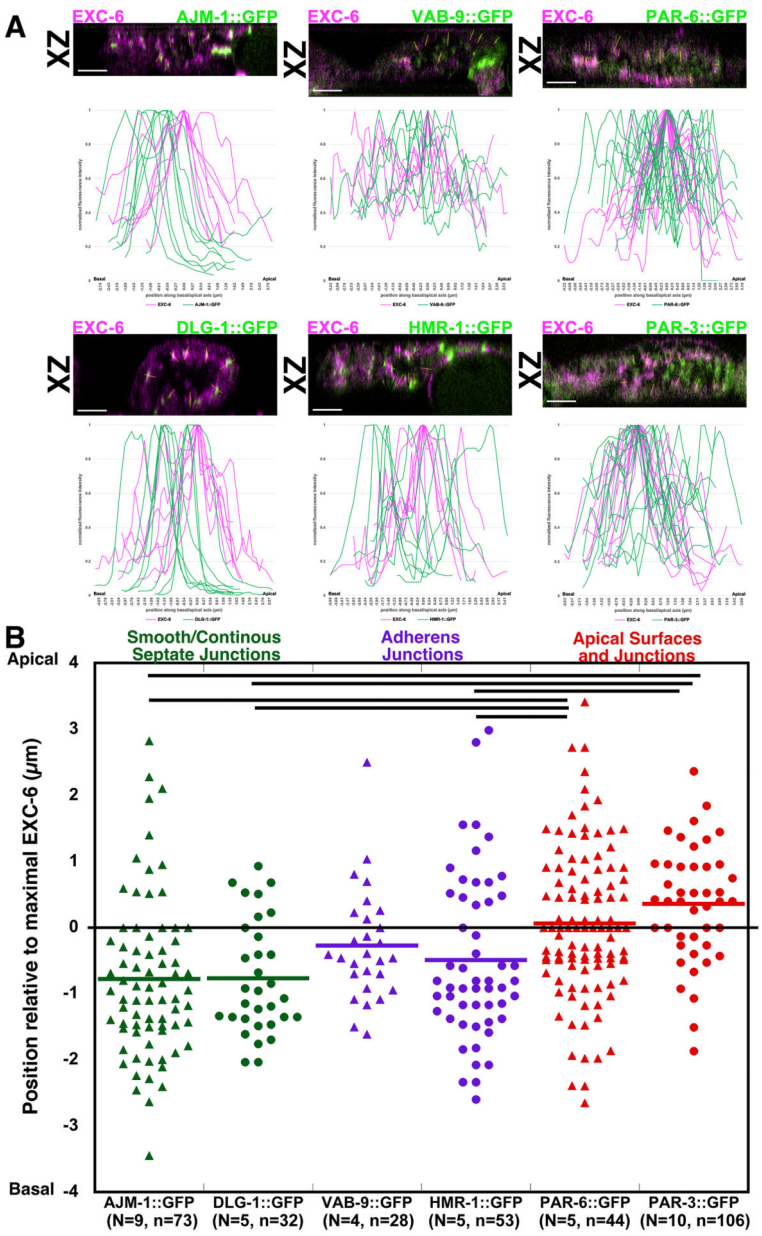

Figure 3.

Measurement of EXC-6 apical/basal position relative to known junction markers tagged with GFP. (A) Confocal sections of representative spermathecae are shown with lines drawn across EXC-6 immunostain and GFP fluorescence signals at cell-cell junctions. Fluorescence intensity values along junctional lines were measured and normalized to a maximum value of 1, and graphed with maximal EXC-6 immunostain positioned at zero, and positions closer to the lumen (i.e. apical) defined as positive, and positions further from the lumen (i.e. basal) as negative. (B) Positions of maximal GFP fluorescence relative to maximal EXC-6 immunostain are shown for measurements at *n* junctions from *N* spermathecae. The average position for smooth/continuous septate junction markers (*green bars*) is basal relative to EXC-6, as is the average position for adherens junction markers

(*purple bars*), while apical marker averages (*red bars*) are either apical or match EXC-6, suggesting EXC-6 associates with the most apical aspect of the spermatheca junctions, likely the pleated septate junctions. All comparisons in relative positions that show statistical significance ($p < 0.05$) are indicated (*black bars*).

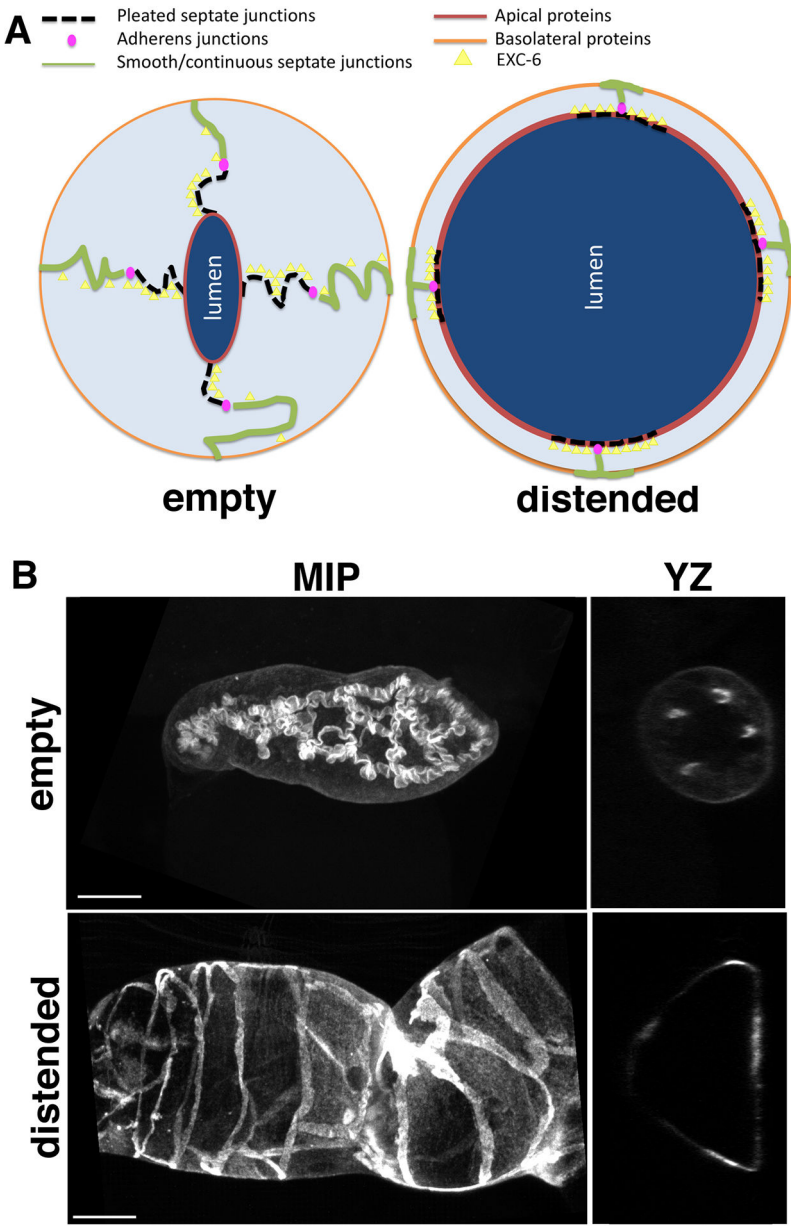

Figure 4.

EXC-6-associated junctions unzip during ovulation. (A) Models of spermathecae cross-sections, comparing an empty spermatheca with one distended during ovulation. The convoluted nature of smooth/continuous and pleated septate junctions in empty spermathecae has been demonstrated (Lints and Hall, 2009). Unzipping of these in the distended spermatheca is hypothesized to occur as a mechanism to accommodate oocyte entry. *Yellow triangles* represent the predicted association of EXC-6 with the pleated septate junctions. (B) Maximum intensity projections (*MIP*) and cross-sections (*YZ*) of empty and distended spermathecae show EXC-6::GFP-associated junctions convert from curly ribbons (observed in *MIP*) with vertical/near vertical orientation relative to the luminal surface

(observed in *YZ*), into straight bands (in *MIP*) that are horizontally-oriented relative to the lumen surface (in *YZ*), indicating junction unzipping during distension. Scale bars, 10 μm.

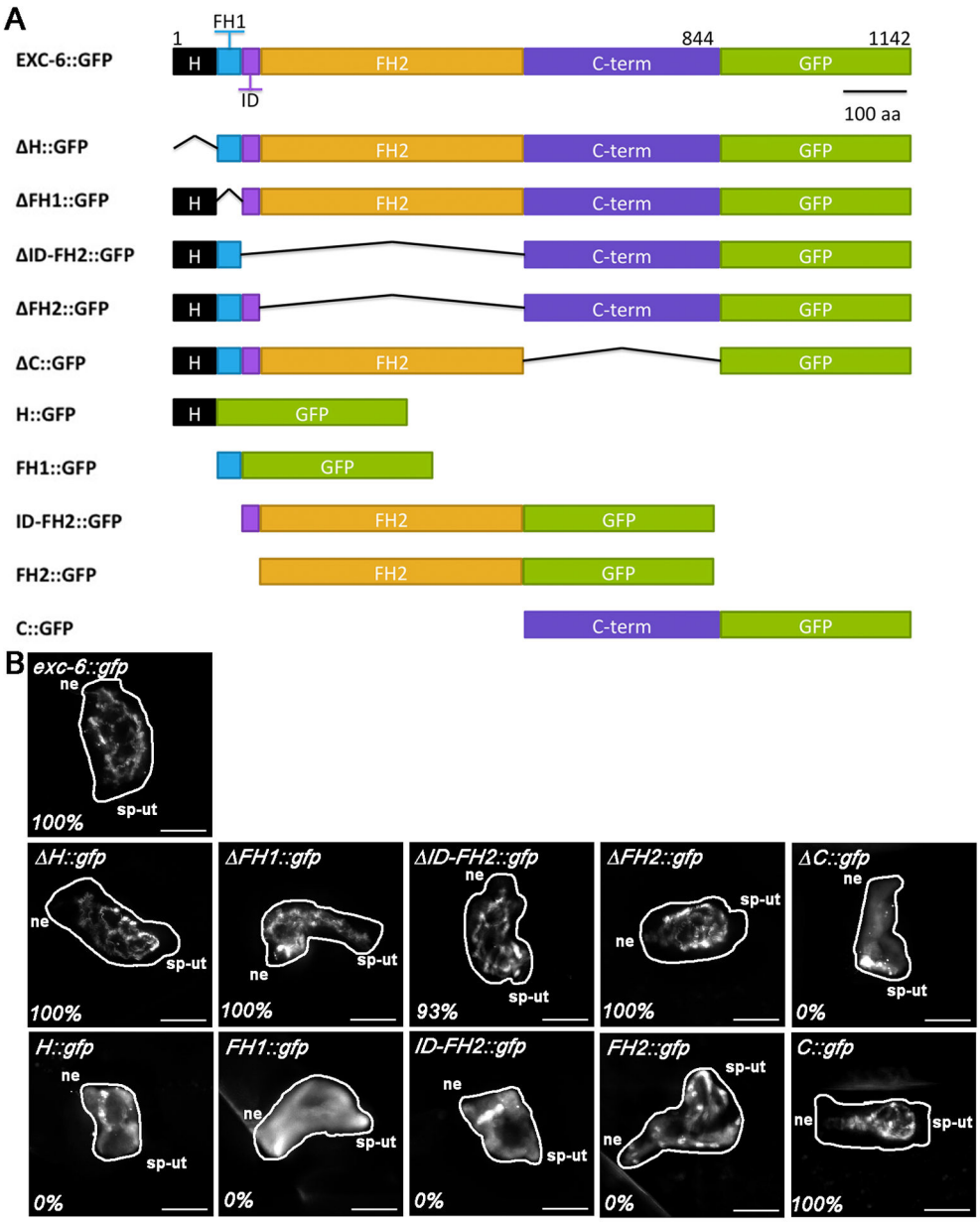

Figure 5.

The EXC-6 C-terminal tail is necessary and sufficient for localization to spermatheca cell-cell junctions. (A) Domain maps of EXC-6::GFP constructs generated, depicting predicted N-terminal helical motif (H), FH1 domain, inter-FH1/FH2-domain region (ID), FH2 domain, and C-terminal tail (C-term). Scale bar, 100 amino acids. (B) Spermathecae expressing indicated fusion constructs in live *exc-6(gk386)* adults. Extent of spermathecae (*white outlines*), and approximate positions of the spermatheca neck (*ne*) adjoining the proximal gonad arm, and of the spermatheca-uterine valve (*sp-ut*) are indicated. Spermathecae are flexible, mobile organs *in vivo*, accounting for the high variability in their orientation, shape and apparent size. Numbers indicate percentages of observed spermathecae with junction-associated GFP, determined from 20 spermathecae for each

construct. Similar percentages were observed in two additional independently isolated transgenic lines for each construct. Scale bars, 20 μm.

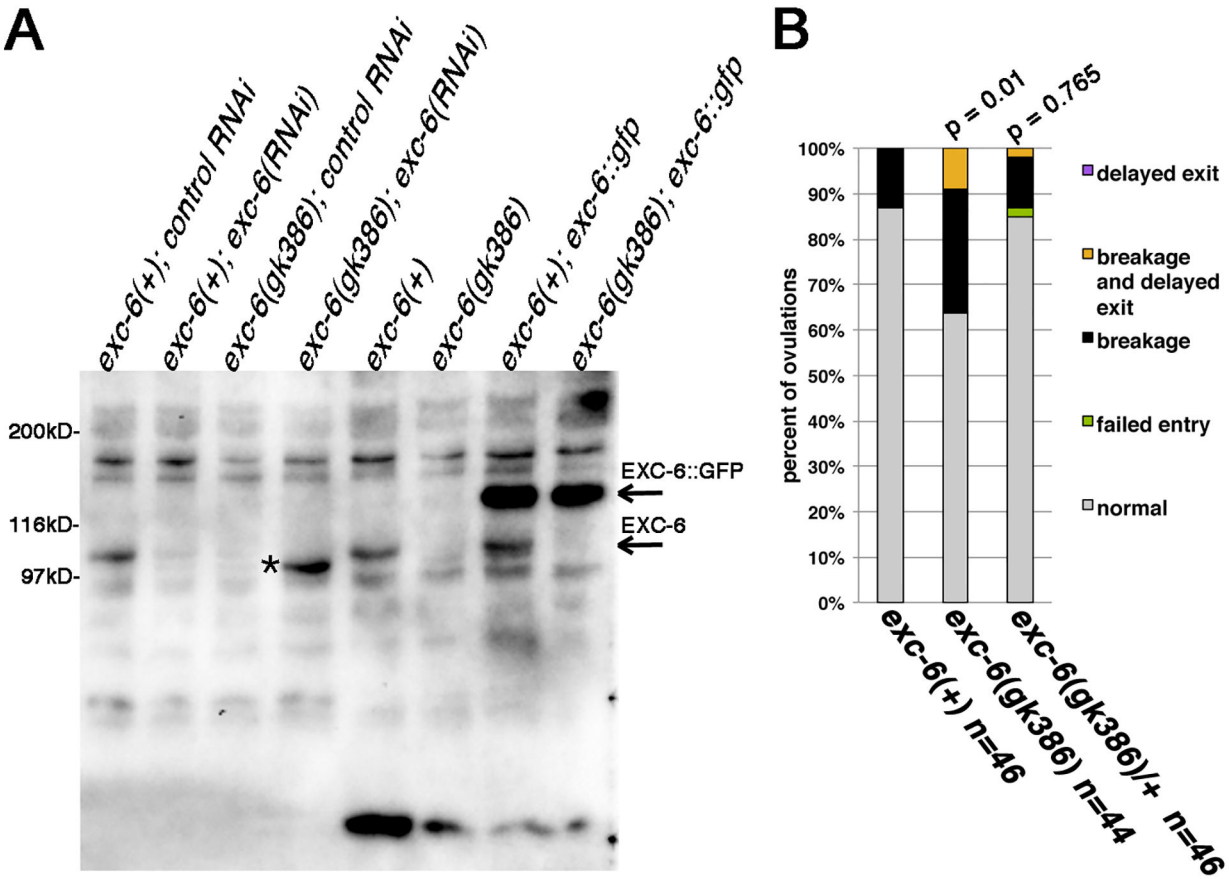

Figure 6.

gk386 is a null allele of *exc-6*. (A) Anti-EXC-6 western blot shows endogenous EXC-6 at ~105 kD is lost from worm extracts after *exc-6(RNAi)* or in *exc-6(gk386)* mutants, while ~ 128 kD EXC-6::GFP in transgenic animals is overexpressed relative to endogenous EXC-6. The band indicated by asterisk (*) is a bacterial antigen (see Supplementary Figure S4). No novel smaller or larger immunoreactive species are detected in *exc-6(gk386)* extracts. (B) Frequencies of ovulation phenotypes in wild-type, homozygous *exc-6(gk386),* and *exc-6(gk386)/(+)* worms show *exc-6(gk386)* behaves as a recessive allele. Shown are the combined results of three experiments. P-values are for comparisons to wild type.

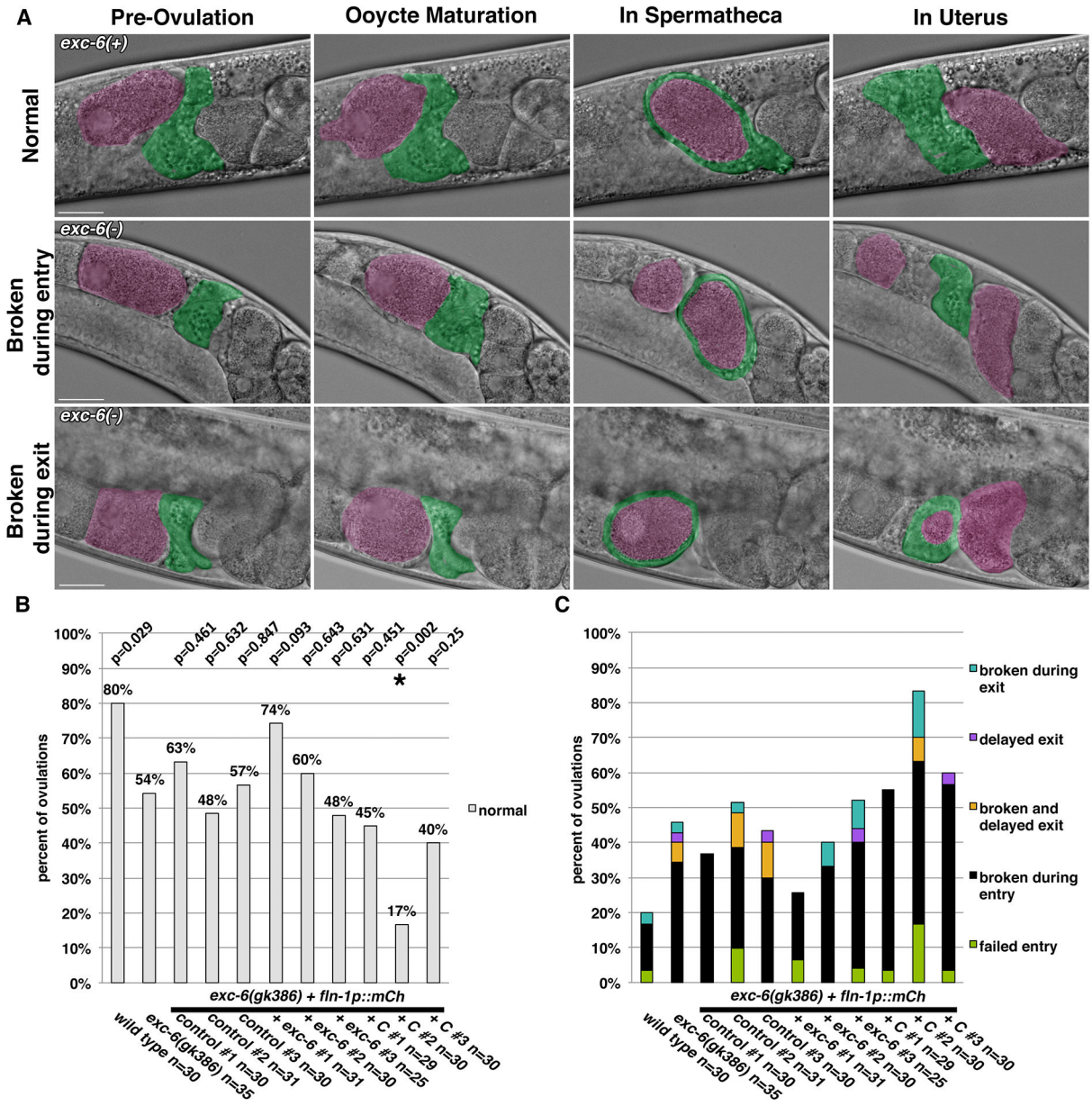

Figure 7.

Ovulation and transit defects in *exc-6(gk386)* worms are exacerbated by the isolated EXC-6 C-terminal tail. (A) Ovulation was monitored in worms by DIC microscopy. Representative images from Supplementary Video S1 show consecutive steps during ovulation. Normally (*top*), a matured oocyte (*magenta*) enters the spermatheca (*green*), is fertilized, and exits to the uterus. Also shown are ovulations in *exc-6(gk386)* animals in which the oocyte is broken during entry (*middle*), or when the fertilized egg is broken during exit (*bottom*). Non-colored images are reproduced in Supplementary Figure S6 for clarity. Scale bars, 20 μm. Percent of observed ovulations that are (B) normal or (C) aberrant, with breakdown of specific phenotypes. P-values shown in (B) are for comparison to *exc-6(gk386)* using the

Bonferroni correct p-value 0.005. * indicates statistical significance when compared to *exc-6(gk386)*. See Supplementary Table S5 for statistical analysis details.

Table 1:

Measured distances along a basal-to-apical axis between maximal EXC-6 immunostain and maximal GFP fluorescence for junction markers shown in Figure 3.

junctionmarker	spermathecae analyzed (#)	junctions analyzed (#)	distance (μm) mean ± SD[†]	neg (#)[‡]	pos (#)[§]	same (#)[¶]
AJM-1	9	73	0.79 ± 1.20	53	16	4
DLG-1	5	32	0.77 ± 0.86	24	7	1
VAB-9	4	28	0.27 ± 0.86	20	7	1
HMR-1	5	53	0.49 ± 1.24	36	16	1
PAR-6	5	44	−0.06 ± 1.13	45	46	11
PAR-3	10	106	−0.36 ± 0.88	13	27	4

[†]Mean measured distance between maximal EXC-6 immunostain and maximal GFP fluorescence ± 1 standard deviation. Positive values reflect apical positioning relative to EXC-6, while negative values reflect basal relative positioning.

[‡]Number of measured junctions that exhibited basal positioning of GFP relative to EXC-6.

[§]Number of measured junctions that exhibited apical positioning of GFP relative to EXC-6.

[¶]Number of measured junctions that exhibited the same apical/basal positioning of GFP relative to EXC-6.